

# Critical-state model for harmonic generation in a superconducting microwave resonator

J. McDonald and John R. Clem

*Ames Laboratory and Department of Physics and Astronomy, Iowa State University, Ames, Iowa 50011*

D. E. Oates

*Lincoln Laboratory, Massachusetts Institute of Technology, Lexington, Massachusetts 02173*

*and Department of Physics, Massachusetts Institute of Technology, Cambridge, Massachusetts 02139*

(Received 18 September 1996)

A critical-state model is developed for the treatment of the nonlinear ac response of a superconducting coaxial-type transmission line. Analytical results are presented for the resistance and reactance as well as the response at overtone frequencies. Center conductors of both elliptical and rectangular thin-film cross section are considered. The dominant response, in the case of the elliptical geometry, is found to be independent of the aspect ratio of the ellipse. Significant differences are found between the elliptical and strip geometries. These differences are due to the difference in structure of the critical state in the two geometries. The model is applied to resonators with the assumption that end effects can be neglected. Qualitative agreement is found with experimental results. [S0163-1829(97)01317-9]

## I. INTRODUCTION

There is presently considerable interest in the use of high-temperature superconductors (HTS's) in passive microwave devices such as filters for wireless communication.<sup>1-4</sup> Many people believe that this will be one of the first widespread applications for HTS's.<sup>1</sup> Recent prototypes of HTS filters have shown performance superior to conventional filters by at least an order of magnitude.<sup>1,3,4</sup> This improvement is due to the lower losses in HTS as compared with conventional metallic conductors such as copper. Lower conductor loss in a resonator translates into a larger  $Q$  and, therefore, a smaller bandwidth. High- $Q$  resonators also provide a convenient method for studying fundamental properties of HTS's. In the Meissner state the reactive part of the surface impedance is proportional to the penetration depth. Therefore, the temperature and field dependence of the surface impedance can yield information about the lower critical field  $H_{c1}$  and about the symmetry of the order parameter.<sup>5</sup> High- $Q$  resonators are also a convenient way of studying vortex dynamics and high-dissipation regimes because large transport currents can be created even at modest input power.

One aspect of HTS's that distinguishes them from conventional conductors, and complicates device design, is their nonlinearity, which manifests itself in a dependence of the surface impedance on the input power or transport current amplitude.<sup>5,6</sup> One consequence of the power dependence is that the low-power surface impedance is no longer a sufficient figure of merit for the material. Instead, the surface impedance must be determined at the specific power at which the device will be operated.<sup>5</sup> Nonlinearities also lead to harmonic generation (HG) and two-frequency intermodulation (IM). The occurrence of IM in filters can cause various problems such as the generation of spurious targets in radar receivers.<sup>5</sup> A thorough understanding of all these effects is essential before high-quality devices can be successfully designed and constructed. While these effects are present even at small input powers, they become much more pronounced

as the power increases. Experimental evidence suggests that the nonlinearity is associated with the onset of vortex penetration and hysteresis.<sup>5,6</sup> Previous modeling of the data has assumed a coupled-grain model at low input power.<sup>2</sup> This model was successful in fitting the behavior of both the resistive and reactive responses of the surface impedance. At higher input powers a modified Bean model was employed.<sup>2</sup> This model was able to quantitatively explain the power dependence of the surface resistance. Sridhar proposed a critical-state model for the resistance and reactance.<sup>7</sup> Thus far, satisfactory models to explain HG and IM in either the low-power or high-power regions have been lacking.<sup>2</sup>

The purpose of this paper is to provide a model, similar to Sridhar's, for describing the power dependence of the surface impedance and HG due to quasistatic vortex penetration and hysteresis. We will employ a field-independent critical-state model with the assumption that  $H_{c1}=0$  (Bean model).<sup>8</sup> This should be an excellent approximation when the average self-field is greater than  $H_{c1}$ . We will also neglect any effects due to surface barriers.<sup>9</sup> A model describing two-frequency IM will be presented in a separate paper.

## II. THE MODEL

We consider a one-dimensional coaxial-type transmission line. The outer conductor is a superconducting cylindrical shell of radius  $R$ . The inner conductor is either a superconducting wire of elliptical cross section with semimajor axis  $a$  and semiminor axis  $b$ , or a superconducting thin-film strip of width  $2W$  and thickness  $d$  (see Fig. 1). The center conductor carries a transport current  $I_T(t)=I_{T0}\cos(\omega_0 t)$ . We assume that for the elliptical geometry  $\lambda \ll a$ , and that for the strip geometry either  $\lambda < d \ll W$  or  $d < \lambda < \Lambda \ll W$ , where  $\lambda$  is the London penetration depth and  $\Lambda=2\lambda^2/d$  is the two-dimensional screening length.<sup>10</sup> We will also assume that  $R$  is large enough that the center conductor can be treated as if it were isolated. It can be shown that this is not a very restrictive assumption.<sup>11-13</sup> These assumptions allow us to use

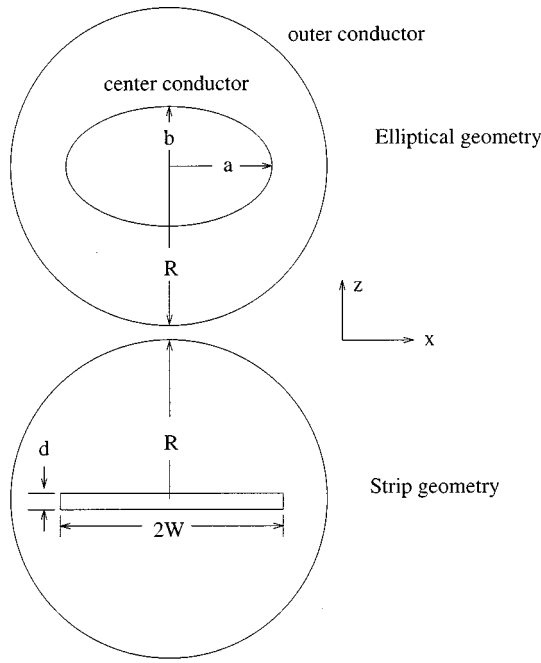


FIG. 1. A sketch of the two geometries considered in this paper. The outer conductor is a cylindrical shell of radius  $R$ . The center conductor is either an elliptical wire with aspect ratio  $\alpha = a/b$  or a thin-film strip of width  $2W$  and thickness  $d$ , where  $a \ll R$  and  $W \ll R$ . The  $y$  axis points into the page.

the well-known results for infinitely long, isolated elliptical wires and strips.<sup>14-16</sup>

When  $I_{T0}$  becomes large enough, vortices will start to penetrate into the center conductor from its surface. In our calculations we assume that  $H_{c1} = 0$  and that there are no surface barriers, so vortex penetration occurs for all  $I_{T0} > 0$ . For simplicity we will neglect any vortex penetration in the outer conductor. We assume that  $\omega_0$  is small enough that we can treat the vortex motion quasistatically. This will be done using a critical-state model with field-independent  $J_c$ .<sup>14-16</sup>

There are significant differences between the critical state in an elliptical wire and that in a strip. As shown in Ref. 14, in an elliptical wire (see Fig. 2) the flux fronts are concentric ellipses (they all have the same aspect ratio  $\alpha = b/a$ ). When the transport current is decreased from its peak value  $I_{T0}$ , there will be three distinct regions in the wire. There is a central region  $|x| < a_0$  which is both flux and current free. The size of this region depends on the ratio of the peak current  $I_{T0}$  to the saturation current  $I_c = \pi a a^2 J_c$ . The middle region  $a_0 < |x| < a_1$  contains frozen-in flux from the previous front. The current density in this region is  $J_y(x) = +J_c$ . The outer region  $a_1 < |x| < a$  is occupied by the new front, and the current density is  $J_y(x) = -J_c$ . Thus, the critical state in an elliptical wire is similar to that in a circular wire.<sup>14</sup> In the case of a strip (see Fig. 3), there is a central region  $|x| < a_0$ , which is shielded from magnetic flux but contains a screening-current density. The middle regions  $a_0 < |x| < a_1$  contain frozen-in flux from the previous front. The current density in these regions is not equal to  $+J_c$  but rather is a function of position. The outer regions  $a_1 < |x| < W$  are occupied by the new front. The current density in these regions is  $J_y(x) = -J_c$ .<sup>15,16</sup>

The voltage drop per unit length  $V(t)$  is given by Faraday's law

$$V(t) = \frac{d}{dt} \left[ \int_0^R dx B_z(x, t) \right], \quad (1)$$

where  $B_z$  is the  $z$  component of the flux density in the  $x$ - $y$  plane. Since  $I_T(t)$  is periodic with period  $T = 2\pi/\omega_0$ ,  $V(t)$  is periodic with the same period. We may, therefore, express  $V(t)$  as a Fourier series

$$V(t) = I_{T0} \sum_{n=1}^{\infty} [R_n \cos(n\omega_0 t) - X_n \sin(n\omega_0 t)], \quad (2)$$

where the coefficients  $R_n$  and  $X_n$  are given by

$$R_n = \frac{\omega_0}{\pi I_{T0}} \int_0^T dt V(t) \cos(n\omega_0 t) \quad (3)$$

and

$$X_n = \frac{-\omega_0}{\pi I_{T0}} \int_0^T dt V(t) \sin(n\omega_0 t), \quad (4)$$

respectively. The dissipated power per unit length is given by

$$P_{\text{diss}} = \frac{1}{T} \int_0^T dt I_T(t) V(t). \quad (5)$$

Inserting Eq. (2) into Eq. (5) yields

$$P_{\text{diss}} = \frac{1}{2} I_{T0}^2 R_1. \quad (6)$$

Equation (6) implies that  $R_1$  is the resistance per unit length.  $X_1$  is the reactance per unit length which is related to the inductance and to the resonant frequency. When  $I_{T0} \rightarrow 0$ ,  $V(t)$  becomes purely inductive; therefore,  $X_1 \rightarrow X_0$  where  $X_0$  is the geometric reactance per unit length. For  $n > 1$ ,  $R_n$  and  $X_n$  yield information on the generation of higher harmonics in the transmission line.

### III. RESULTS

#### A. Elliptical geometry

We will first consider the case where the center conductor has an elliptical cross section. The expressions for  $a_0$ ,  $a_1$ , and  $B_z$  can be derived from the results of Norris.<sup>14</sup> The expressions for  $a_0$  and  $a_1$  are

$$a_0 = a \sqrt{1 - F} \quad (7)$$

and

$$a_1(t) = \begin{cases} a \sqrt{1 - F \sin^2(\omega_0 t/2)}, & 0 < t < T/2, \\ a \sqrt{1 - F \cos^2(\omega_0 t/2)}, & T/2 < t < T, \end{cases} \quad (8)$$

where  $F = I_{T0}/I_c$ . The expressions for  $B_z$  are given in Appendix A. If the expressions for  $B_z$  are used in Eq. (1) the result is

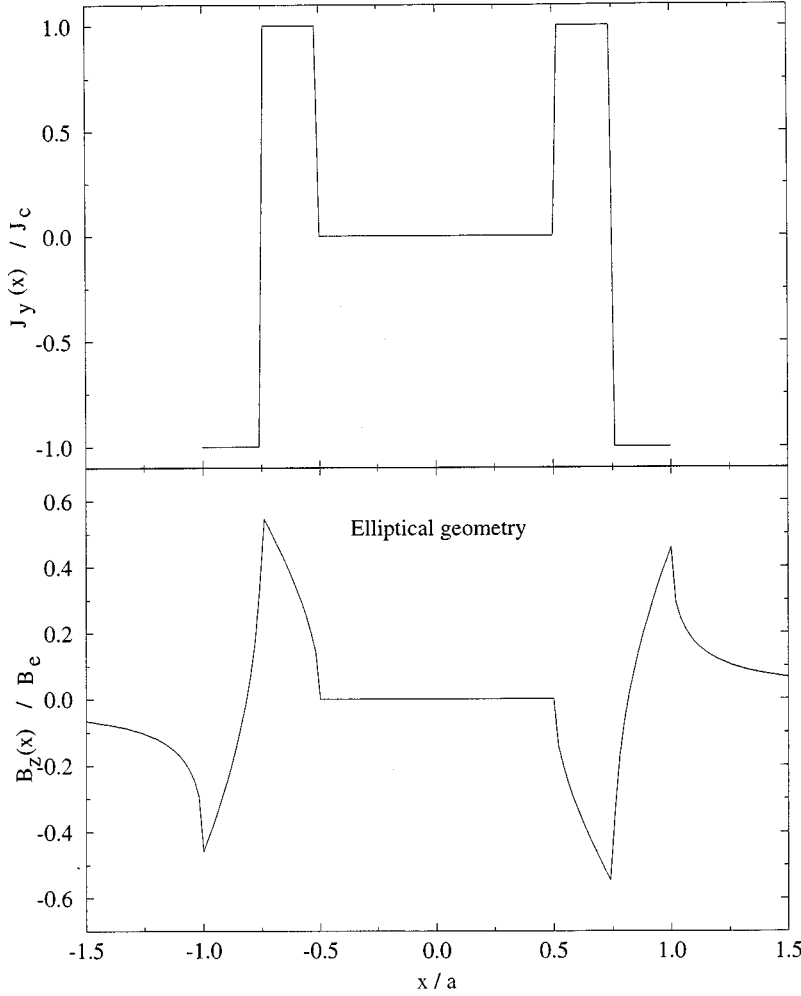


FIG. 2. The critical state for an elliptical wire upon decreasing the transport current from the peak value  $I_{T0}$ . There is a central region  $0 < x < a_0$  in which both the current density and flux density vanish. There is a middle region  $a_0 < x < a_1$  carrying a current density  $J_y(x) = +J_c$  and an outer region  $a_1 < x < a$  carrying a current density  $J_y(x) = -J_c$ . There is a nonzero flux density in both the middle and outer regions. In the case shown,  $a_0 = 0.5a$  and  $a_1 = 0.75a$ .

$$V(t) = -I_{T0} \frac{\mu_0 \omega_0}{2\pi} \sin(\omega_0 t) \ln \left( \frac{R + \sqrt{R^2 - (1 - \alpha^2) a_1(t)^2}}{(1 + \alpha) a_1(t)} \right). \quad (9)$$

The logarithm can be expanded around large  $R$  to obtain

$$V(t) = I_{T0} \frac{\mu_0 \omega_0}{2\pi} \sin(\omega_0 t) \left\{ -\ln \left( \frac{2}{(1 + \alpha)} \frac{R}{a} \right) + \ln \left( \frac{a_1(t)}{a} \right) + O \left[ \left( \frac{a_1(t)}{R} \right)^2 \right] \right\}. \quad (10)$$

The first and largest term is the voltage drop per unit length in the absence of vortex penetration ( $I_{T0} \rightarrow 0$ ). The second term is the dominant term arising from the quasistatic vortex penetration. It is interesting to note that this term is independent of  $\alpha$ . The third term leads to small corrections and will be neglected.

Using Eqs. (3) to calculate  $R_1$ , we find

$$R_1 = \frac{\mu_0 \omega_0}{2\pi} \frac{1}{\pi F^2} [F(2 - F) + 2(1 - F) \ln(1 - F)]. \quad (11)$$

Inserting Eq. (11) into Eq. (6), we obtain Norris' result for the losses in an elliptical wire<sup>14</sup>

$$P_{\text{diss}} = \frac{\omega_0}{2\pi} \frac{\mu_0 I_c^2}{\pi} [F(1 - F/2) + (1 - F) \ln(1 - F)]. \quad (12)$$

Using Eq. (4) to calculate  $X_1$  we obtain

$$X_1 = X_0 + \Delta X_1, \quad (13)$$

where  $\Delta X_1$  is given by

$$\Delta X_1 = \frac{\mu_0 \omega_0}{4\pi} \left[ -\frac{1}{2} + \frac{2\sqrt{1 - F}(2 - F - 2\sqrt{1 - F})}{F^2} - \ln \left( \frac{2 - F + 2\sqrt{1 - F}}{4} \right) \right] \quad (14)$$

and

$$X_0 = \frac{\mu_0 \omega_0}{2\pi} \ln \left( \frac{2}{(1 + \alpha)} \frac{R}{a} \right). \quad (15)$$

$\Delta X_1$  is the power-dependent or nonlinear part of the reactance, while  $X_0$  is the geometric reactance.

The coefficients for all higher harmonics can be calculated analytically. For the even harmonics it is found that

$$R_{2n} = X_{2n} = 0. \quad (16)$$

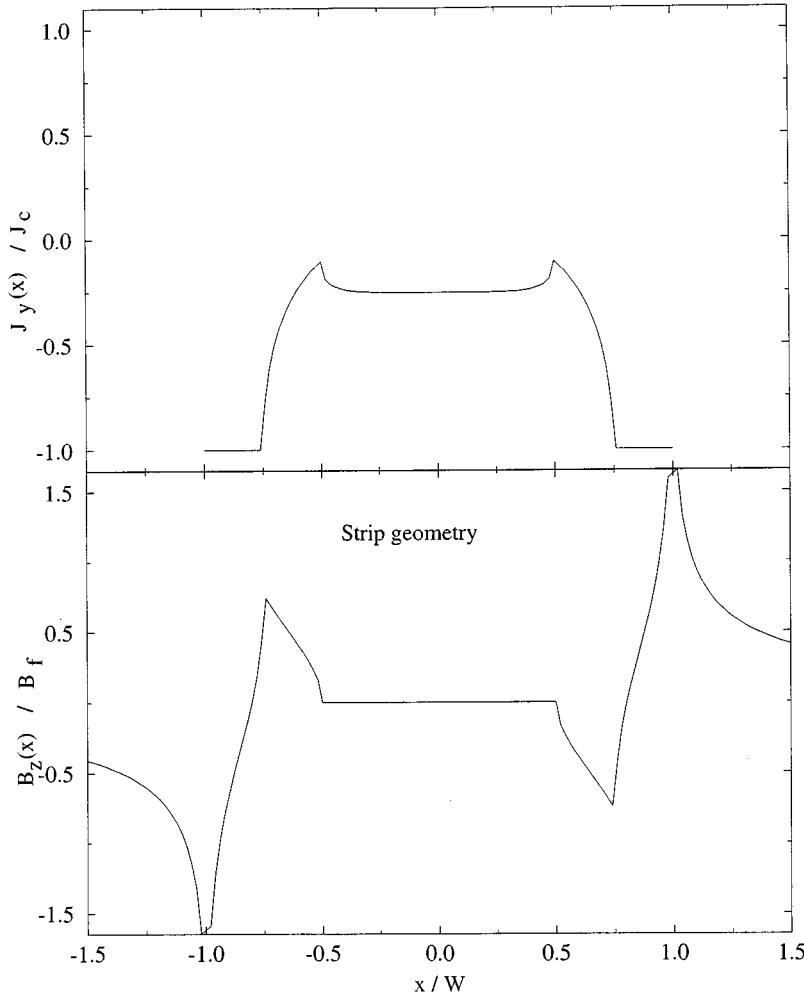


FIG. 3. The critical state in a thin-film strip upon decreasing the transport current from the peak value  $I_{T0}$ . There is a central region  $|x| < a_0$  where the flux density vanishes but not the current density. There is a middle region in which the current density is not equal to  $+J_c$  but rather is a function of position (the expression is given in Appendix A), and there is an outer region where the current density is  $J_y(x) = -J_c$ . There is a nonzero flux density in both the middle and outer regions. In the case shown,  $a_0 = 0.5a$  and  $a_1 = 0.75a$ .

The expressions for  $R_3$  and  $X_3$  are given in Appendix B. The expressions for the higher harmonic coefficients are lengthy and have, therefore, been omitted.

For  $F \ll 1$ , the leading-order behaviors of  $R_1$ ,  $\Delta X_1$ ,  $R_3$ , and  $X_3$  are given by

$$R_1 = \frac{\mu_0 \omega_0}{2\pi} \frac{F}{3\pi}, \quad (17)$$

$$\Delta X_1 = \frac{\mu_0 \omega_0}{4\pi} \frac{F}{2}, \quad (18)$$

$$R_3 = \frac{\mu_0 \omega_0}{2\pi} \left( -\frac{F}{5\pi} \right), \quad (19)$$

$$X_3 = \frac{\mu_0 \omega_0}{2\pi} \frac{F^2}{64}. \quad (20)$$

### B. Strip geometry

We next consider the case where the center conductor is a thin-film strip. The expressions for  $a_0$  and  $a_1$  are

$$a_0 = W\sqrt{1-F^2}, \quad (21)$$

and

$$a_1(t) = \begin{cases} W\sqrt{1-F^2} \sin^4(\omega_0 t/2), & 0 < t < T/2, \\ W\sqrt{1-F^2} \cos^4(\omega_0 t/2), & T/2 < t < T. \end{cases} \quad (22)$$

The expressions for  $B_z$  (Refs. 15 and 16) are given in Appendix A. If the expressions for  $B_z$  are used in Eq. (1), the result is

$$V(t) = -I_{T0} \frac{\mu_0 \omega_0}{2\pi} \sin(\omega_0 t) \ln \left( \frac{R + \sqrt{R^2 - a_1(t)^2}}{a_1(t)} \right). \quad (23)$$

The logarithm can be expanded around large  $R$  to obtain

$$V(t) = I_{T0} \frac{\mu_0 \omega_0}{2\pi} \sin(\omega_0 t) \left\{ -\ln \left( \frac{2R}{W} \right) + \ln \left( \frac{a_1(t)}{W} \right) + O \left[ \left( \frac{a_1(t)}{R} \right)^2 \right] \right\}. \quad (24)$$

The third term is a small correction and will be neglected. The expressions for  $R_1$  and  $X_1$  are found to be

$$R_1 = \frac{\mu_0 \omega_0}{2\pi} \frac{2}{\pi F^2} [(1+F) \ln(1+F) + (1-F) \ln(1-F) - F^2], \quad (25)$$

which yields Norris' result for the losses in a thin-film strip<sup>14</sup>

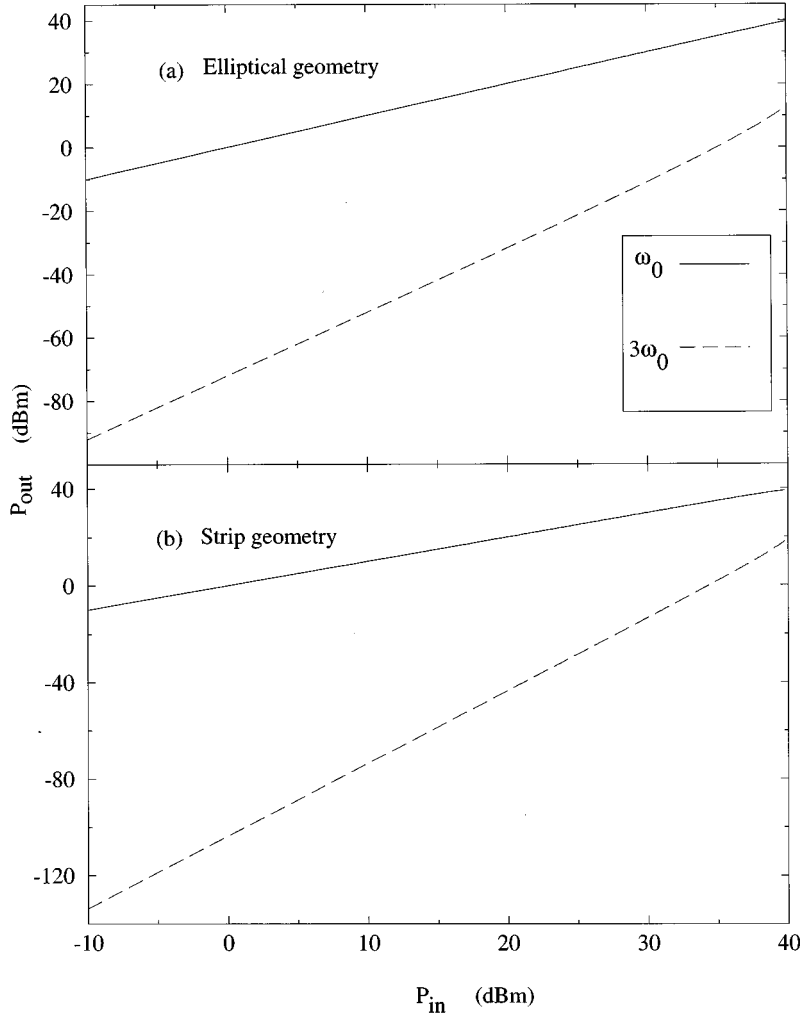


FIG. 4. Response of a resonator, with either an elliptical (a) or strip (b) center conductor, at frequencies  $\omega_0$  and  $3\omega_0$ . The parameter values used were  $Z_0 = 50 \, \Omega$ ,  $f_0 = \omega_0/2\pi = 1.6 \, \text{GHz}$ ,  $\ell = 3 \, \text{cm}$ ,  $W$  or  $a = 75 \, \mu\text{m}$ ,  $d$  or  $2b = 0.3 \, \mu\text{m}$ , and  $J_c = 10^6 \, \text{A/cm}^2$ . It was assumed that the dielectric constant characterizing the region between the conductors is  $\epsilon = 10$ .

$$P_{\text{diss}} = \frac{\omega_0}{2\pi} \frac{\mu_0 I_c^2}{\pi} [(1+F) \ln(1+F) + (1-F) \ln(1-F) - F^2] \quad (26)$$

and

$$X_1 = X_0 + \Delta X_1, \quad (27)$$

where  $\Delta X_1$  is given by

$$\Delta X_1 = -\frac{\mu_0 \omega_0}{4\pi} \left[ 1 + \frac{2[4 - (2-F)\sqrt{1-F} - (2+F)\sqrt{1+F}]}{F^2} + \ln \left( \frac{(2-F+2\sqrt{1-F})(2+F+2\sqrt{1+F})}{16} \right) \right], \quad (28)$$

and

$$X_0 = \frac{\mu_0 \omega_0}{2\pi} \ln \left( \frac{2R}{W} \right). \quad (29)$$

The coefficients for the higher harmonics can be calculated analytically. The even harmonics vanish:

$$R_{2n} = X_{2n} = 0. \quad (30)$$

The expressions for  $R_3$  and  $X_3$  are given in Appendix B.

The leading-order behaviors for  $F \ll 1$  are

$$R_1 = \frac{\mu_0 \omega_0}{2\pi} \frac{F^2}{3\pi}, \quad (31)$$

$$\Delta X_1 = \frac{\mu_0 \omega_0}{4\pi} \left( \frac{5F^2}{16} \right), \quad (32)$$

$$R_3 = \frac{\mu_0 \omega_0}{2\pi} \left( -\frac{F^2}{5\pi} \right), \quad (33)$$

$$X_3 = \frac{\mu_0 \omega_0}{2\pi} \frac{F^2}{32}. \quad (34)$$

#### IV. COMPARISON WITH EXPERIMENT

Resonators have a finite length. Therefore, if we want to apply our results to a resonator, we must assume that the fringing effects due to the ends of the resonator can be neglected, and our expressions for  $V(t)$ ,  $R_n$ ,  $X_n$ , and  $P_{\text{diss}}$  must be multiplied by the resonator length to make them dimensionally correct. It can be shown that for a resonator of length  $\ell$ ,  $X_0$  is related to the characteristic impedance  $Z_0$  by  $\ell X_0 = \pi Z_0$ . In a typical experiment a current with amplitude  $I_{T0}$  is established in the center conductor. The output voltage signal is analyzed to determine the distribution of power among the various frequencies inside the resonator. The

amount of output power at a given frequency can then be plotted versus the input power to determine the degree of nonlinearity in the resonator. The expression for the time-averaged available incident power  $P_{\text{inc}}$  in terms of the peak current  $I_{T0}$  is  $P_{\text{inc}} \approx (1/2)I_{T0}^2/\mathcal{X}_0$ . The relation between the time-averaged output power  $P_{\text{out}}$  and  $P_{\text{inc}}$  is given by  $P_{\text{out}} = r_v^2 P_{\text{inc}}$ , where  $r_v$  is the voltage insertion ratio. In terms of  $S$  parameters,  $r_v = |S_{21}|$ . The insertion loss (IL) is given by  $\text{IL} = -20 \log_{10} r_v$  dB. In HG measurements a well-matched transmission-line sample is used.<sup>4</sup> Therefore, the IL is primarily determined by  $P_{\text{diss}}$  and not by coupling loss. Therefore, the time-averaged input power  $P_{\text{in}}$  is given by  $P_{\text{in}} = P_{\text{inc}}$ , and  $P_{\text{out}}$  is given by  $P_{\text{out}} = P_{\text{in}} - P_{\text{diss}}$ . The output power is distributed among the various harmonics. The power spectrum at frequency  $n\omega_0$  is proportional to  $R_n^2 + X_n^2$ . The amount of output power at frequency  $n\omega_0$  [ $P_{\text{out}}(n\omega_0)$ ] is given by the product of the time-averaged output power and the fraction of power stored at that frequency,

$$P_{\text{out}}(n\omega_0) = P_{\text{out}} \times \left( \frac{R_n^2 + X_n^2}{\sum_{n'=1}^{\infty} (R_{n'}^2 + X_{n'}^2)} \right). \quad (35)$$

Figure 4 shows plots of  $P_{\text{out}}(\omega_0)$  and  $P_{\text{out}}(3\omega_0)$  versus  $P_{\text{in}}$  for both the elliptical and strip geometries. The slope of the  $P_{\text{out}}(\omega_0)$  versus  $P_{\text{in}}$  curve is equal to one for both geometries. The slope of the  $P_{\text{out}}(3\omega_0)$  versus  $P_{\text{in}}$  curve is equal to two in the elliptical geometry and equal to three in the strip geometry. It can be shown that the third-order intercept (TOI) for the elliptical geometry is given by

$$P_{\text{in}}^{(\text{TOI})} = \frac{1}{2} \left( \frac{5\pi I_c}{\mu_0(\omega_0/2\pi)\mathcal{L}} \right)^2 (\pi Z_0)^3. \quad (36)$$

For the strip geometry the TOI is given by

$$P_{\text{in}}^{(\text{TOI})} = \frac{(\pi I_c Z_0)^2 / [\mu_0(\omega_0/2\pi)\mathcal{L}]}{2\sqrt{(1/5\pi)^2 + (1/32)^2}}. \quad (37)$$

Using the parameter choices  $Z_0 = 50 \Omega$ ,  $f_0 = \omega_0/2\pi = 1.6$  GHz,  $\mathcal{L} = 3$  cm,  $W$  or  $a = 75 \mu\text{m}$ ,  $d$  or  $2b = 0.3 \mu\text{m}$ , and  $J_c = 10^6$  A/cm<sup>2</sup>, the TOI, defined as  $10 \log_{10}[P_{\text{in}}^{(\text{TOI})}/mW]$  dBm, is equal to +72.2 dBm for the elliptical geometry and +57.7 dBm for the strip geometry.

The values of the TOI calculated from Eq. (37) are in reasonable agreement with experimental values for coplanar *TBCCO* lines given in Table II of Ref. 20, although the ground plane and dielectric geometries are different. A better way to compare our theory to experiment, however, is to examine how the TOI depends on line width, line length, and temperature, as was done in Table III of Ref. 20. According to Eq. (37), the change in the TOI when only the width of the line is changed from  $2W_1$  to  $2W_2$  is  $\Delta \text{TOI} = 20 \log_{10}(W_2/W_1)$ . When only the length of the line changes from  $\mathcal{L}_1$  to  $\mathcal{L}_2$ , the corresponding TOI difference is  $\Delta \text{TOI} = 10 \log_{10}(\mathcal{L}_1/\mathcal{L}_2)$ , and when only the temperature is changed from  $T_1$  to  $T_2$ , then  $\Delta \text{TOI} = 20 \log_{10}[J_c(T_2)/J_c(T_1)]$ . Table I shows a comparison of experimental<sup>20</sup> and theoretical values for  $\Delta \text{TOI}$ . Excellent agreement between theory and experiment is found with regard to the width dependence, and fair agreement is found with the dependencies on length and temperature.

TABLE I. Comparison of the theoretical and experimental results for  $\Delta \text{TOI}$  as the width, length, and temperature are varied independently. The experimental values were taken from Ref. 20. The values for the critical current density at a given temperature were determined by taking the average of all accurately reported values at that temperature.

Parameter	$\Delta \text{TOI}$ (dBm)	
	Experiment	Theory
Width ( $W \rightarrow 2W$ )	6.2	6.0
( $W \rightarrow 4W$ )	12.2	12.0
( $W \rightarrow 8W$ )	18.4	18.1
Length (14 mm $\rightarrow$ 1 mm)	9.7	11.5
(14 mm $\rightarrow$ 5 mm)	3.1	4.5
(5 mm $\rightarrow$ 1 mm)	6.5	7.0
Temperature (100 K $\rightarrow$ 90 K)	15.6	12.3
(90 K $\rightarrow$ 80 K)	5.4	3.1
(80 K $\rightarrow$ 70 K)	5.5	5.8

The ratio  $r = (\Delta\omega_0/\omega_0)/\Delta(1/2Q)$  has been stressed as an important figure of merit characterizing the nonlinearity in resonators.<sup>6,17-19</sup> This quantity can be determined experimentally from the resonance curve.  $\Delta\omega_0$  is the shift in position of the peak of the curve, and  $Q$  is the reciprocal of the bandwidth. This ratio is also related to the theoretical quantities  $R_1$  and  $\Delta X_1$ . The change in the bandwidth  $\Delta(1/Q)$  is given by

$$\Delta\left(\frac{1}{Q}\right) = \frac{R_1}{X_1}, \quad (38)$$

and the relative shift in resonant frequency  $\Delta\omega_0/\omega_0$  is given by

$$\frac{\Delta\omega_0}{\omega_0} = \frac{1}{2} \frac{\Delta X_1}{X_1}. \quad (39)$$

Substituting these expressions into the expression for  $r$  yields

$$r = \frac{\Delta X_1}{R_1}. \quad (40)$$

Therefore,  $r$  provides a simple way to compare experiment and theory.

In Nb microstrip resonators, the quantity  $r$  was found to be essentially constant ( $\sim 1$ ) except at temperatures close to  $T_c$ .<sup>6</sup> In this case a plot of  $\Delta\omega_0/\omega_0$  versus  $\Delta(1/2Q)$  should be a straight line with slope of order unity at smaller values of  $F$ , and should deviate from a straight line at larger  $F$  values. Figure 5 shows such a plot using our expressions for  $R_1$  and  $\Delta X_1$ .

A frequency-independent  $r$  value of order unity is characteristic of the nonlinearity caused by vortex pinning and hysteresis. For other mechanisms the magnitude and frequency dependence of the  $r$  value may be quite different.<sup>18,19,21</sup> For the case of the low-field behavior of weak links, the  $r$  value is often one or two orders of magnitude larger and is inversely proportional to the

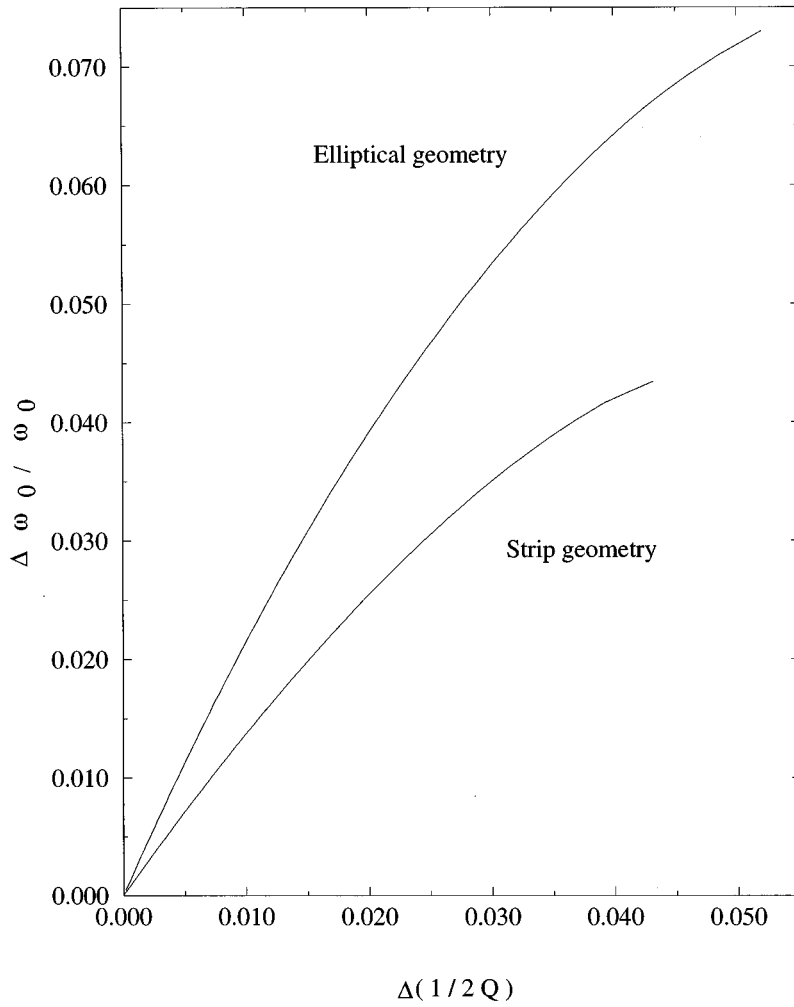


FIG. 5. Plot of  $\Delta\omega_0/\omega_0$  vs  $\Delta(1/2Q)$  for a resonator with an elliptical or strip center conductor. The curves end at  $F=1$ . The initial slopes of the lines, corresponding to  $F \ll 1$ , are 2.4 and 1.5 for the ellipse and strip, respectively. This straight-line behavior is observed experimentally.

frequency.<sup>18,19,21</sup> This has been observed in granular and polycrystalline samples in small fields.<sup>21</sup>

## V. SUMMARY

We have presented a critical-state model for the nonlinear ac response of a superconducting coaxial-type transmission line. This model can be applied to superconducting microwave resonators if fringing effects due to the resonator ends are neglected. Center conductors of both elliptical and thin-film cross section were treated. For the elliptical geometry the results were found to be independent of the aspect ratio of the ellipse. For small currents the impedance in the elliptical geometry was found to be proportional to the current amplitude, while in the strip geometry it was found to be proportional to the square of the current amplitude. Analytical formulas were derived for the input power at the third-order intercept for harmonic generation. These results should be relevant to experiments dealing with the design and testing of superconducting microwave resonators and filters.

## ACKNOWLEDGMENTS

Ames Laboratory is operated for the U.S. Department of Energy by Iowa State University under Contract No. W-7405-Eng-82. This research was supported by the Direc-

tor for Energy Research, Office of Basic Energy Sciences. The work at M.I.T. was supported by the Air Force Office of Scientific Research, and by DARPA.

## APPENDIX A: FLUX DENSITY AND CURRENT DENSITY EXPRESSIONS

The expressions for  $J_y(x)$  and  $B_z$ , for the case of an elliptical geometry, are

$$J_y(x) = \begin{cases} 0, & 0 < x < a_0, \\ +J_c, & a_0 < x < a_1, \\ -J_c, & a_1 < x < a, \end{cases} \quad (\text{A1})$$

and

$$B_z(x) = \begin{cases} 0, & 0 < x < a_0, \\ -B_e \left( \frac{x/a}{1+\alpha} - f(a_0) \right), & a_0 < x < a_1, \\ -B_e \left( 2f(a_1) - f(a_0) - \frac{x/a}{1+\alpha} \right), & a_1 < x < a, \\ -B_e (2f(a_1) - f(a) - f(a_0)), & a < x < R, \end{cases} \quad (\text{A2})$$

where the function  $f$  is given by

$$f(u) = \frac{(u/a)^2}{x/a + \sqrt{(x/a)^2 - (1 - \alpha^2)(u/a)^2}}, \quad (\text{A3})$$

and the scaling field  $B_e$  is defined as

$$B_e = \mu_0 \alpha J_c a. \quad (\text{A4})$$

For the case of the strip geometry the expressions are

$$J_y(x) = \begin{cases} \frac{2J_c}{\pi} \left[ \tan^{-1} \left( \sqrt{\frac{W^2 - a_0^2}{a_0^2 - x^2}} \right) - 2 \tan^{-1} \left( \sqrt{\frac{W^2 - a^2}{a^2 - x^2}} \right) \right], & 0 < x < a_0, \\ J_c \left[ 1 - \frac{4}{\pi} \tan^{-1} \left( \sqrt{\frac{W^2 - a^2}{a^2 - x^2}} \right) \right], & a_0 < x < a_1, \\ -J_c, & a_1 < x < W, \end{cases} \quad (\text{A5})$$

and

$$B_z(x) = \begin{cases} 0, & 0 < x < a_0, \\ -B_f \ln \left( \frac{\sqrt{W^2 - x^2}}{\sqrt{W^2 - a_0^2} - \sqrt{x^2 - a_0^2}} \right), & a_0 < x < a_1, \\ -B_f \left[ \ln \left( \frac{\sqrt{|x^2 - W^2|}}{|\sqrt{x^2 - a_0^2} - \sqrt{W^2 - a_0^2}|} \right) - 2 \ln \left( \frac{\sqrt{|x^2 - W^2|}}{|\sqrt{x^2 - a^2} - \sqrt{W^2 - a^2}|} \right) \right], & a < x < R, \end{cases} \quad (\text{A6})$$

where the scaling field  $B_f$  is defined by

$$B_f = \frac{\mu_0 J_c d}{\pi}. \quad (\text{A7})$$

## APPENDIX B: COEFFICIENTS FOR THIRD HARMONIC RESPONSE

The expressions for  $R_3$  and  $X_3$  for the case of an elliptical geometry are

$$R_3 = \frac{\mu_0 \omega_0}{2\pi} \frac{1}{3\pi F^4} \{ 48F - 72F^2 + 22F^3 + F^4 + [48(1 - F) + 6F^2](1 - F) \ln(1 - F) \}, \quad (\text{B1})$$

and

$$X_3 = \frac{\mu_0 \omega_0}{2\pi} \frac{1}{8F^4} [F^4 + 16F^3 - 144F^2 + 256F - 128 + 64(2 - F)\sqrt{(1 - F)^3}]. \quad (\text{B2})$$

For the case of strip geometry the expressions are

$$R_3 = \frac{\mu_0 \omega_0}{2\pi} \frac{1}{3\pi F^4} [2F^4 - 144F^2 + [48(1 + F) + 6F^2] \times (1 + F) \ln(1 + F) + [48(1 - F) + 6F^2] \times (1 - F) \ln(1 - F)], \quad (\text{B3})$$

and

$$X_3 = \frac{\mu_0 \omega_0}{2\pi} \frac{1}{4F^4} [F^4 - 144F^2 - 128 + 32(F^2 - 3F + 2)\sqrt{1 - F} + 32(2 + F)\sqrt{(1 + F)^3}]. \quad (\text{B4})$$

<sup>1</sup>G. B. Lubkin, Phys. Today **48**, 20 (1995).

<sup>2</sup>D. E. Oates, P. P. Nguyen, G. Dresselhaus, M. S. Dresselhaus, G. Koren, and E. Polturak, J. Supercond. **8**, 725 (1995).

<sup>3</sup>G. -C. Liang, D. Zhang, C. -F. Shih, M. E. Johansson, R. S. Withers, W. Ruby, D. E. Oates, A. C. Anderson, P. A. Polakos, P. M. Mankiewich, E. DeObaldia, and R. E. Miller, IEEE Trans. Micro. Th. Tech. **43**, 3020 (1995).

<sup>4</sup>Z. -Y. Shen, *High-Temperature Superconducting Microwave Circuits* (Artech House, Boston, 1994).

<sup>5</sup>P. P. Nguyen, D. E. Oates, G. Dresselhaus, M. S. Dresselhaus,

and A. C. Anderson, Phys. Rev. B **51**, 6686 (1995).

<sup>6</sup>M. A. Golosovsky, H. J. Snortland, and M. R. Beasley, Phys. Rev. B **51**, 6462 (1995).

<sup>7</sup>S. Sridhar, Appl. Phys. Lett. **65**, 1054 (1994).

<sup>8</sup>C. P. Bean, Phys. Rev. Lett. **8**, 250 (1962).

<sup>9</sup>J. R. Clem, J. Appl. Phys. **50**, 3518 (1979).

<sup>10</sup>J. Pearl, Appl. Phys. Lett. **5**, 65 (1964).

<sup>11</sup>A. M. Campbell, IEEE Trans. Appl. Supr. **5**, 687 (1995).

<sup>12</sup>S. Fleshler, L. T. Cronis, G. E. Conway, A. P. Malozemoff, T. Pe, J. McDonald, J. R. Clem, G. Vellego, and P. Metra, Appl. Phys.



- Lett. **67**, 3189 (1995).
- <sup>13</sup>J. R. Clem, M. Benkraouda, T. Pe, and J. McDonald, Chin. J. Phys. **34**, 284 (1996).
- <sup>14</sup>W. T. Norris, J. Phys. D **3**, 489 (1970).
- <sup>15</sup>E. H. Brandt and M. Indenbom, Phys. Rev. B **48**, 12 893 (1993).
- <sup>16</sup>E. Zeldov, J. R. Clem, M. McElfresh, and M. Darwin, Phys. Rev. B **49**, 9802 (1994).
- <sup>17</sup>J. Halbritter, Part. Accel. **3**, 163 (1972).
- <sup>18</sup>J. Halbritter, J. Appl. Phys. **68**, 6315 (1990).
- <sup>19</sup>J. Halbritter, J. Supercond. **8**, 691 (1995).
- <sup>20</sup>C. Wilker, Z. -Y. Shen, P. Pang, W. L. Holstein, and D. W. Face, IEEE Trans. Appl. Supr. **5**, 1665 (1995).
- <sup>21</sup>J. Halbritter (unpublished).